The correlation between N deficiency and the mechanical properties of the Ti2AlNy MAX phase

Yu Wenbo, Wenzhe Jia, Feng Guo, Zhaoyang Ma, Pengcheng Zhang, Christophe Tromas, Véronique Gauthier-Brunet, Paul R.C. Kent, Weiwei Sun, Sylvain Dubois

The correlation between N deficiency and the mechanical properties of the Ti_2AlN_y MAX phase

Wenbo Yu[1*], Wenzhe Jia[1], Feng Guo[1], Zhaoyang Ma[1], Pengcheng Zhang[1], Christophe Tromas[3], Véronique Gauthier-Brunet[3], Paul R. C. Kent [2,4], Weiwei Sun[2*], Sylvain Dubois[3]

1. Center of Materials Science and Engineering, School of Mechanical and Electronic Control Engineering, Beijing Jiaotong University, Beijing 100044, China

2. Center for Nanophase Materials Sciences, Oak Ridge National Laboratory, Oak Ridge, Tennessee 37831, United States

3. Institute PPRIME, Département de Physique et Mécanique des Matériaux, CNRS-Université de Poitiers -ENSMA, Boulevard Marie et Pierre Curie, TSA 41123, 86073 Poitiers Cedex 9, France

4. Computational Sciences and Engineering Division, Oak Ridge National Laboratory, Oak Ridge, Tennessee 37831, United States

Abstract:

The role of X deficiency on the mechanical properties of MAX phases was studied by synthesizing Ti_2AlN by powder metallurgy in stoichiometric and sub/extra-stoichiometric nitrogen compositions. XRD analyses and *ab initio* calculations indicate that nitrogen vacancies result in a lattice contraction predominantly along the *c*-axis. The elastic moduli and intrinsic hardness of substoichiometric $Ti_2AlN_{0.9}$ measured from nanoindentation tests are shown to be slightly smaller than that of Ti_2AlN. The key mechanical indexes, bulk (*B*), shear (*G*) and Young's (*E*) moduli as well as the hardness variation are calculated in density functional theory, and show different responses depending on the concentration of N vacancies. This joint experimental and theoretical study provides a full understanding of the energetics, chemical bonding, electronic structure, and mechanics of the N deficient MAX phases which would increase the application of nitride ceramics.

Keywords: Nonstoichiometric Ti_2AlN; Anisotropic; Microstructure; Mechanical properties;

*Dr. W. Yu: wbyu@bjtu.edu.cn

*Dr. W. Sun: provels8467@gmail.com

1. **Introduction**‡

MAX phases denoted as $M_{n+1}AX_n$ (n=1-3) are a class of layered hexagonal ternary carbides/nitrides, where M is an early transition metal, A is from group IIIA or IVA element, X is C and/or N. MAX phases exhibit a combination of strong covalent M-X bonds interleaved with A layers through weak M-A bonds.[1, 2] In sharp contradiction with binary carbides/nitrides (hard and brittle, nonmachinable, damage intolerant, and susceptible to thermal shock), MAX phases exhibit machinability, excellent electrical and thermal conductivities, thermal shock and oxidation resistance, stiffness at high temperature and self-lubrication capacity, which bridge the gap between metals and ceramics [2-8]. Ti-based MAX phase compounds are used as ohmic contacts on wide-gap semiconductors to achieve high-quality of electronic devices [9, 10], and have shown good tolerance to neutron irradiation[11].

Concerning the crystal structure, MAX phases and MX phases have similar Ti-N and Ti-C chemical bonding characteristics[12]. In binary transition metal carbide/nitrides, mechanical, chemical and physical properties can be modified by controlling the vacancies in X site (TiC_x (x=0.5-0.98) and TiN_y (y=0.6-1.1) [12-14]). The introduction of 12.5% of vacancies in TiN has been shown to reduce shear stiffness from 190 GPa to about 150GPa.[15]However, very few studies related to the X deficiency exist for ternary carbides/nitrides MAX phases, possibly due to the difficulty of controlling the defect concentration compared with the binary TiC/TiN.[14] For example, Yu at al. reported that the synthesis of pure Ti_2AlC can only be achieved with the 2Ti:1.05Al:0.85C nominal composition by hot isostatic pressing (HIP) at 1400°C/80MPa for 4h. Guo et al. [16] demonstrated that single-phased Ti_2AlC_x (x<1) can be fabricated by combustion synthesis starting with 2Ti:Al:0.7C powder

mixture. The main combustion product is Ti_3AlC_2 if the molar ratio of the reactant mixture is 2Ti:Al:C. Cabioc'h et al. reported that a large nitrogen deficiency in Ti_2AlN can be realized[17], which provides with an effective means to investigate the effect of X site vacancies on the microstructure and properties of MAX phases. Substoichiometric effects allow modifying and, in some cases, improving their physical properties. For example, Scabarozi et *al.* have shown that substoichiometric $Ti_2AlN_{0.95}$ has a higher resistivity than stoichiometric Ti_2AlN[18] which suggests that vacancies are strong electron scatters.

The MAX phases are also of interest because the ability to etch away the A atoms enables the synthesis of two-dimensional MXenes.[2, 19] Notably, nitride MXenes are predicted to exhibit higher capacitance than carbides as the promising capacitive materials[20], but they have not been widely studied. The control of the N deficiency in MAX phases would thus result in new MXenes.

In the present work, a series of Ti_2AlN_y MAX phases in a wide N concentration (y=0.85-1.05) are synthesized by pressureless sintering. The cell parameters, octahedral and trigonal distortion parameters are determined both by the Rietveld method and calculated by *ab initio* calculations as a function of the vacancy content. Nanoindentation is used to evaluate intrinsic hardness and elastic moduli of $Ti_2AlN_{0.9}$ and Ti_2AlN synthesized by hot isostatic pressing. In order to interpret the experiments, theoretical calculations were performed to determine the N vacancy energetics, the impact on the chemical bonding and electronic structure, and on the mechanical properties. The pioneering correlation between the defects on the X site and the atomic-scale understanding would lay fundamental understanding on this nitride MAX.

2. Experimental details

Powders of Ti (150-250µm, 99.5% purity), Al (45-150µm, 99.5% purity) and AlN (10µm, 98% purity) were used to synthesize stoichiometric and sub/extra-stoichiometric Ti_2AlN_y. In order to study the effect of N content on Ti_2AlN_y lattice parameters, the samples were produced, from different nominal compositions (2Ti:1.05Al:1.05N, 2Ti:1.05Al:1.0N, 2Ti:1.05Al:0.95N, 2Ti:1.05Al:0.90N and 2Ti:1.05Al:0.85N), by pressureless sintering at 1400°C for 0.5h. To investigate the

vacancy effect on X site, on the intrinsic hardness and indentation modulus values, 2Ti:1.05Al:1.0N and 2Ti:1.05Al:0.90N nominal compositions were used and dense samples were produced by hot isostatic pressing (HIP) at 1400°C/80MPa for 4h. The synthesis procedure is detailed in [21]. The powder mixtures used in this study contain an excess of 5 at.% of Al to compensate the loss of aluminum by preferential out-diffusion during the sintering process.

Samples used for nanoindentation tests were thus grinded using SiC paper and then polished with a diamond suspension. Finally, a chemo-mechanical polishing has been performed using a neutral suspension of alumina nanoparticles. Such a chemo-mechanical polishing allows to produce a very flat surface and to avoid any work hardening due to conventional grinding.

Phase identification was performed by X-Ray Diffraction (XRD) using a Bruker D501 diffractometer with Cu-Kα radiation. XRD data were refined using the MAUD software [30] in order to extract the lattice parameters of the Ti_2AlN_y compounds. Microstructures were examined by Scanning Electron Microscopy (SEM, JEOL 5600LV). Wavelength Dispersive x-ray Spectroscopy (WDS, CAMECA SX100) was used to determine the composition of Ti_2AlN_y resulting from HIP treatment.

Nanoindentation tests have been performed using a Nano Hardness Tester (NHT) apparatus (CSM instrument, Switzerland) equipped with a Berkovich indenter. The indenter shape has been carefully calibrated for true penetration depth as small as 20nm both by direct Atomic Force Microscopy (AFM) observation and by indenting fused silica samples with a Young's modulus of 72GPa. A large indentation network of 150 indents was performed for each sample in order to probe different crystal grain orientations. The load-penetration depth curves are recorded for each nanoindentation test, and the hardness and elastic modulus are determined from the elastic unloading curve using the equivalent indenter method[22, 23]. Different loads (1, 2, 3, 6, 10, 15, 30, 100 mN) corresponding to different penetration depths were used in order to study the hardness variation with penetration depth. SEM observations were carried out to remove from the statistics the hardness and elastic modulus values that have been measured on indents that were not localized on a single MAX phase grain.

3. Theoretical methods

Our theoretical work used density functional theory (DFT) and the Vienna atomic simulation package (VASP)[24-26]. We used the projector augmented wave method (PAW) and the generalized gradient approximation (GGA) Perdew-Burke-Ernzerhof functional [27]. The valence electronic configurations were $2s^2 2p^3$ for N, $3s^2 3p^1$ for Al, and $3p^6 3d^3 4s^1$ for Ti. Geometry optimization utilized 520 eV for the plane wave cutoff energy and convergence criteria of 5×10^{-6}eV for the total energy and 0.01eV/Å^{-1} for the absolute maximum force. Γ centered 15×15×1 ***k***-point grids for Brillouin zone (BZ) integration gave convergence to approximately 3 meV/atom. The special quasi-random structure (SQS) method[28] was employed to describe N deficient structures in 4×4×1 supercells containing 128 atoms. 5×5×1 ***k***-point grids were used for these cells. Unless otherwise noted, all lattice parameters and atomic positions were fully relaxed self-consistently. The Electron Localization Function (ELF)[29, 30] was calculated from the Kohn Sham orbitals.

The stress–strain method was employed to compute elastic constants, c_{ij}. Related mechanical properties were calculated on the basis of the these properties (in Voigt approximation[31]).. The bulk modulus, B and shear modulus, G and Young's modulus, E of polycrystalline aggregates are derived by :

$$G_V = \frac{1}{15}((2c_{11} + c_{33} - c_{12} - 2c_{13}) + \frac{1}{5}(2c_{44} + c_{66}))$$

$$B_V = \frac{2}{9}\left(c_{11} + c_{12} + 2c_{13} + \frac{1}{2}c_{33}\right)$$

$$E = \frac{9BG}{3B + G}$$

4. Results and discussion

4.1 Microstructural characterizations

Fig.1(a-e) shows the back-scattered microstructural morphologies of Ti_2AlN_y fabricated by pressureless sintering at 1400°C for 0.5h from 2Ti:1.05Al:yN (y=0.85,0.9,0.95,1.0 and 1.05) nominal compositions. We can distinguish that the Ti_2AlN grain size decreased with increasing N content in the starting powders. For all samples, EDS analyses show that the overall Ti/Al ratio is 2:0.99, very close to 2:1, which indicates the loss of approximately 5 at.% of the aluminum during reactive

sintering. Starting with 2Ti:1.05Al:0.85N nominal composition [Fig.1(a)], titanium aluminide (Ti_xAl_y) is detected in addition to the desired Ti_2AlN_y MAX phase. Starting with 2Ti:1.05Al:0.9N [Fig.1(b)], 2Ti:1.05Al:0.95N [Fig.1(c)], and 2Ti:1.05Al:1.0N [Fig. 1(d)] nominal compositions, only Ti_2AlN_y is observed; no impurities are detected. Starting with 2Ti:1.05Al:1.05N nominal composition [Fig.1(e)], SEM observations coupled with EDS analyses confirm that Ti_4AlN_y (Ti/Al=4), Ti_2AlN_y (Ti/Al=2) and some Al_2O_3 (white dots) are formed. XRD results confirm SEM/EDS analyses. Indeed, XRD pattern shown in Fig.1(f) demonstrates that only Ti_2AlN_y peaks are detected for N content in the range 0.9-1.0. In addition to Ti_2AlN_y, titanium aluminides (Ti_xAl_y) and Ti_4AlN_y are respectively detected starting with 2Ti:1.05Al:0.85N and 2Ti:1.05Al:1.05N nominal compositions.

Comparing the XRD patterns, the XRD peak corresponding to (006) planes progressively shifts towards higher 2θ values when N content (y) increases, while the (100) peak shift is less significant. In reference to the interplanar spacing calculation in hexagonal system shown in Equation 1,interplanar spacings (d) for (006) and (100) planes are $c/8$, and $3a/4$, respectively.

$$d = \frac{1}{\frac{4}{3}\sqrt{\frac{(h^2 + hk + k^2)}{a^2} + \frac{l^2}{c^2}}} \quad (1)$$

Herein, we find that N vacancy has a stronger effect on the *c* lattice parameter than on *a*

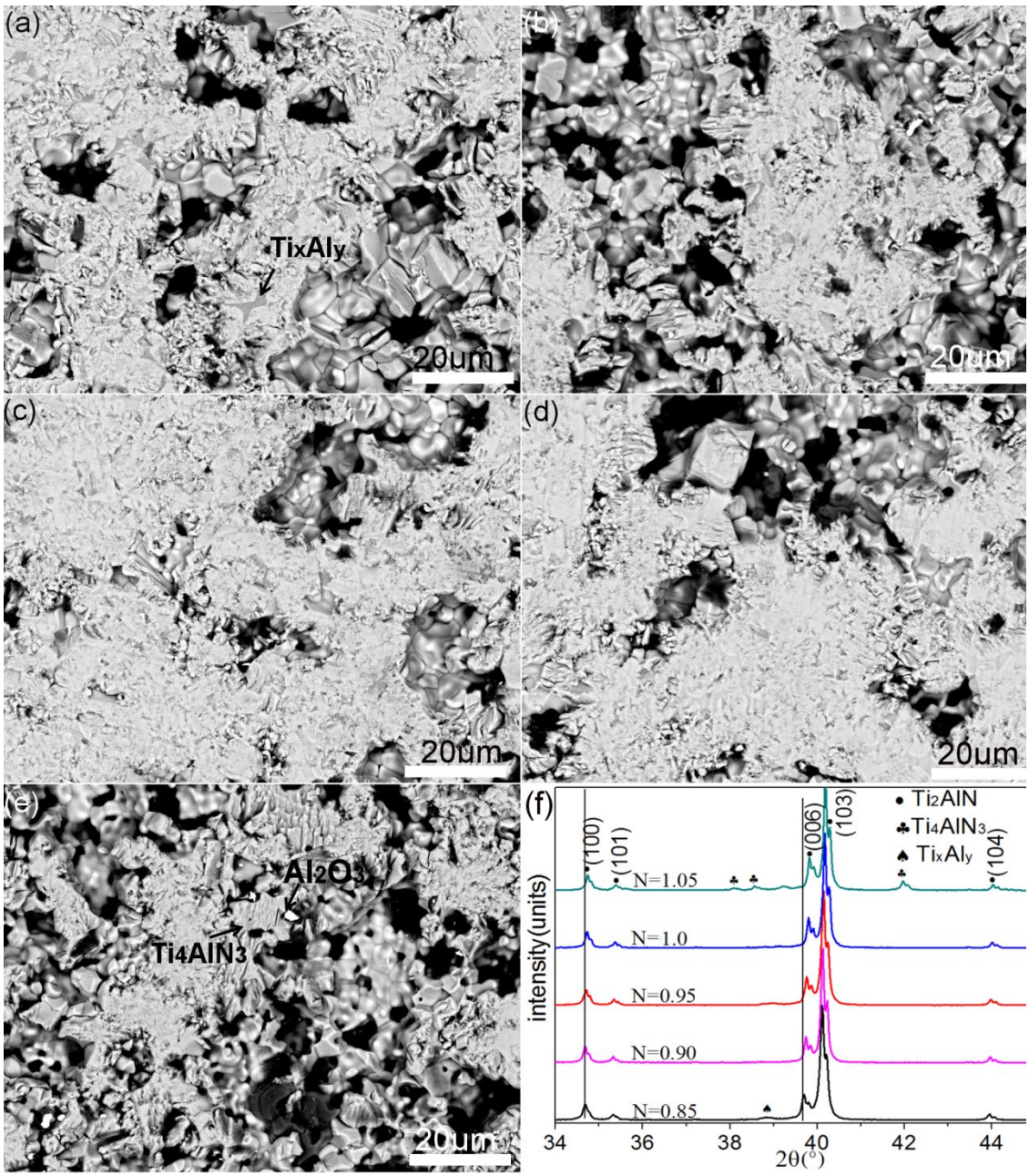

Fig.1: (a-e) Morphologies of Ti_2AlN_y samples produced by pressureless sintering at 1400°C for 0.5h from 2Ti:1.05Al:yN (y=0.85,0.9,0.95,1.0 and 1.05) nominal compositions; (f) XRD patterns of different mixtures sintered at 1400°C for 0.5h. The (hkl) indexed peaks correspond to the Ti_2AlNy MAX phase.

The lattice parameters (LPs) of Ti_2AlN_y as a function of N content, measured from Rietveld refinement of the XRD data using MAUD software, and calculated using ab initio calculations, are summarized in Table I and shown in Fig. 2a. Similar to the findings by Cabioch et al.[17], the volumes of the unit cell remain almost constant independent of y, while different variations for *a* and *c* LPs are clearly found: both experimentally and theoretically, the lattice contraction of Ti_2AlNy is strongly

anisotropic, namely, *a* parameter slightly increases about 0.0062 Å while *c* parameter decreases about 0.0488 Å as the N content increases from 0.85 to 1.05. From Fig. 2b, the variation of the *c*/*a* ratio (about 0.56%) as a function of N content and consistency with the calculations indicates that the N vacancies are primarily randomly distributed. The calculated trends of the LPs well reproduce the experimental measurements.

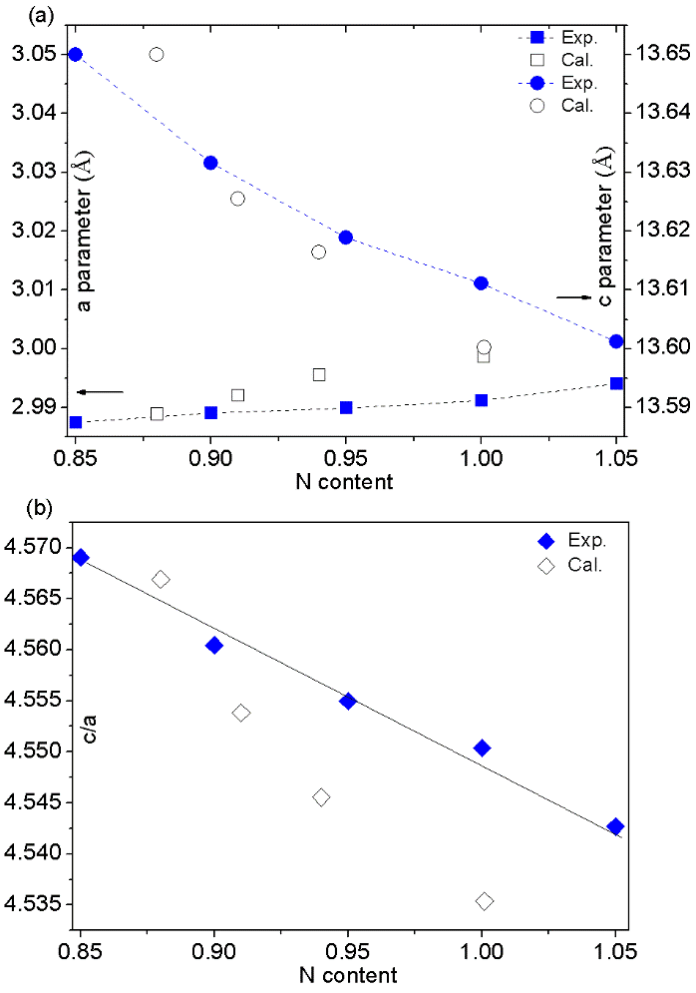

Fig.2. (a) Variation of the *a* and *c* -LPs as a function of nitrogen content in the Ti_2AlN_y compounds from XRD experiments (blue) and *ab initio* calculations (white). (b) the *c*/*a* ratio versus N content. Error bars for lattice parameters being too small to be clearly observable (Uncertainties of 5×10^{-4} Å and 5×10^{-3} Å was typically obtained for a and c parameters.

The MAX crystal unit cell, as shown in Fig.3a, can be considered as constituted of $[M_6X]$ octahedrons and $[M_6A]$ trigonal prisms[32, 33] allowing us to describe the "211" MAX phases[34]. A cubic octahedron is the unit block of the binary MX, but the fourfold axis is absent in ternary MAX that results in a relaxation owing to the lowered

symmetry. The parameter O_d, defined as the ratio of the distances between two faces not in the basal planes (d_1) and two opposite faces contained in the basal planes (d_2)[33], can be used to estimate the non-cubic distortion of the octahedron. It is given by:

$$O_d = \frac{d_1}{d_2} = \frac{\sqrt{3}}{2\sqrt{4Z_{Ti}^2(\frac{c}{a})^2 + \frac{1}{12}}} \quad (2)$$

The distortion parameter P_d, defined as the ratio of the M-M distance and the M-A distance[32], allows estimating the distortion of the trigonal prism. It is given, in either 211 or 312 MAX phases, by:

$$P_d = \frac{1}{\sqrt{(\frac{1}{4} - Z_{Ti})^2(\frac{c}{a})^2 + \frac{1}{3}}} \quad (3)$$

For an ideal packing of hard spheres of equal diameter, a ratio for c/a as of $8\times\sqrt{\frac{2}{3}}$ will be satisfied, and for an ideal octahedron (cubic) and trigonal prism, a unity for both O_d and P_d should also be reached. From the position of Ti atoms (Z_{Ti}), a and c lattice parameters measured above, both O_d and P_d were experimentally determined and plotted as a function of the N content in Ti_2AlN_y in Fig.3b. Obviously, the relative distortion of the prism is similar to the one of the octahedron whatever the N content in Ti_2AlN_y, and the variations of O_d and P_d are very weakly dependent on the N content, and showing the linearly increasing with the N content in both calculations and experiments. The underestimation of O_d and vice versa for P_d might be due to the typical under-bonding of PBE functional in DFT. As shown in Table 1, the distance of Ti-Al monotonically decreases with the increase of N content, but the variation of Ti-N distance is not evident, indicating the different interactions between TiN and Al (weak) as well as the Ti and N (weak). To clarify how the N deficiency inside of Ti_6C octahedra impacts the Ti-Al & Ti-C bond as well as mechanical properties, we carry out the following work.

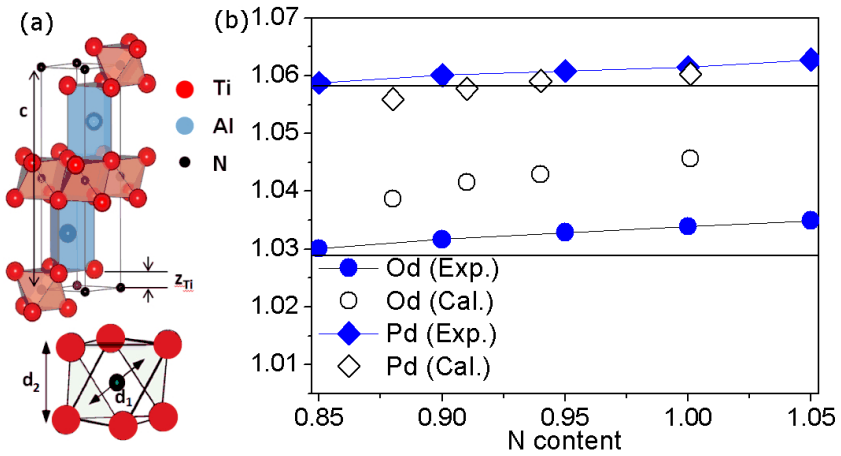

Fig. 3: (a) The unit cell of the Ti_2AlN phase with [Ti_6N] octahedrons (red) and [Ti_6Al] trigonal prisms (blue) represented with VESTA [34]. (b) the Octahedron (O_d, circles) and trigonal prism (P_d, squares) distortion parameters versus N content in Ti_2AlN_y.

4.2 Hardness and Young's moduli

To investigate the influence of N vacancies on Ti_2AlN_y mechanical properties, nanoindentation tests were conducted on samples HIPed from 2Ti:1.05Al:0.9N (Fig.4a) and 2Ti:1.05Al:1.0N (Fig.4b) nominal compositions. WDS analysis indicates that the chemical composition of the Ti_2AlN_y end-products is similar to the starting powders composition. The Al_2O_3 content, determined by image analysis (from ImageJ software) is about 2vol.% starting with 2Ti:1.05Al:1.0N nominal composition and close to 0 starting with 2Ti:1.05Al:0.9N. Here, the Al_2O_3 content decreases with the decrease of the AlN content in the initial reactant powder mixture. Thus, the presence of alumina is likely resulting from the oxidation of AlN starting powders.

Fig.4c shows the variation of the intrinsic hardness and elastic modulus as a function of the indenter penetration depth for $Ti_2AlN_{0.9}$ and $Ti_2AlN_{1.0}$ compounds. The standard deviations result from an average over different grain orientations. From Fig. 4c, one can notice that hardness values strongly decrease with increasing penetration depth. Such an Indentation Size Effect (ISE) [35] was also observed in Ti_3SnC_2[36], Ti_3AlC_2[37] and $Ti_3(Al_{0.8}Sn_{0.2})C_2$[37] MAX phase materials. From Fig. 4c, Ti_2AlN_y nanoindentation modulus remains constant whatever is the penetration depth: the elastic modulus values of $Ti_2AlN_{0.9}$ and Ti_2AlN are respectively 268±10 GPa and 278±10 GPa. Such a result demonstrates that the indenter shape calibration is correct

and, consequently, that the ISE discussed above is not an artefact due to errors in indenter shape calibration.

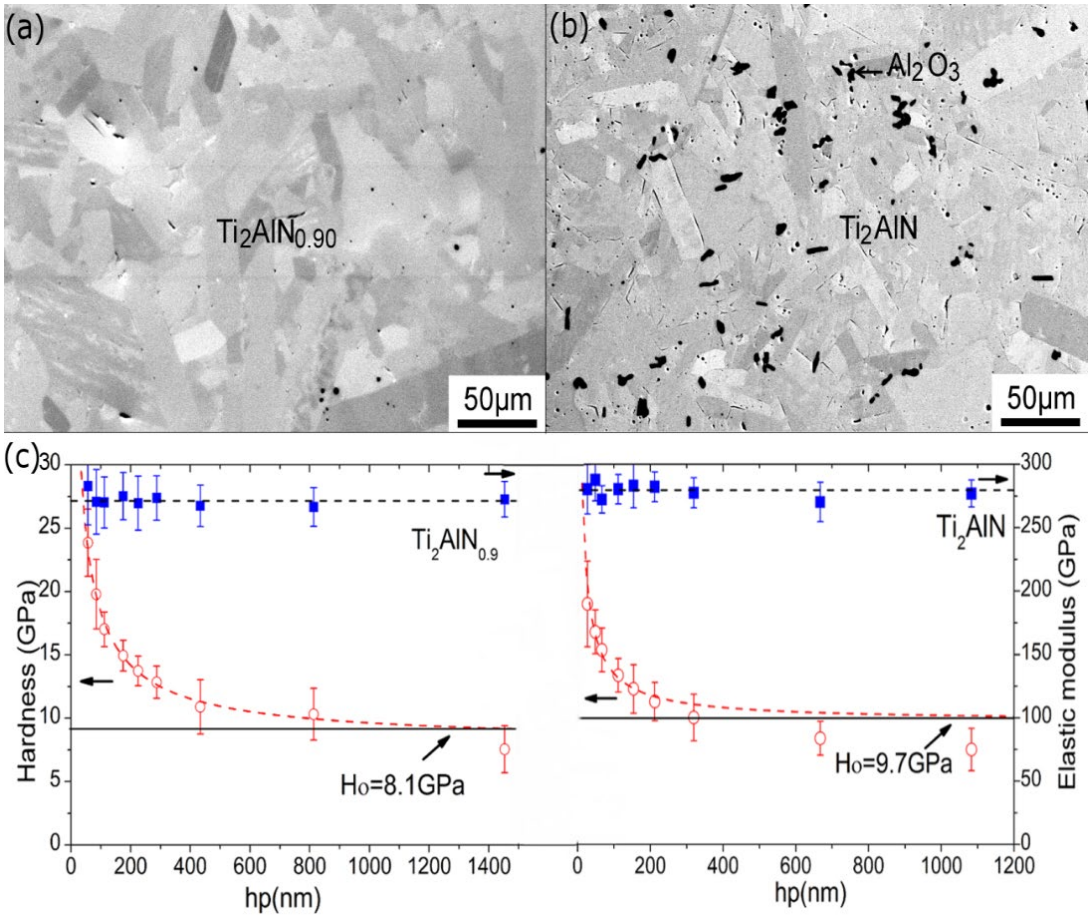

Figure 4: Typical back-scattered images of $Ti_2AlN_{0.90}$ (a) and Ti_2AlN (b) samples HIPed at 1400°C and 80MPa for 4 h from 2Ti:1.05Al:0.90N and 2Ti:1.05Al:1.0N. Hardness (circles) and nanoindentation modulus (squares) of Ti_2AlN and $Ti_2AlN_{0.9}$ (c) as a function of the indenter penetration depth. The red dotted line fits the ISE using the function proposed in the Nix and Gao model[38].

The variation of the hardness values is well-fitted by the same function as that proposed in the Nix and Gao model [38], except for the higher load (i.e.: 100 mN). From the fit shown in Fig. 4c, one can deduce that the intrinsic hardness values of $Ti_2AlN_{0.9}$ and Ti_2AlN are respectively 8.1 and 9.7 GPa. For the 100 mN load, the size of the indents is in the order of the mean grain size. In that case, several grains are involved in the deformation process and grain boundaries play an important role in macroscopic deformation, as reported by Tromas et *al.* [36]. For such high loads, nanoindentation conditions (loads, depth of the indent, number of grains involved in

the deformation,…) are close to microindentation ones and the hardness values are similar to those reported in microindentation experiments.[39]

Up to now, the effect of vacancies on the mechanical properties of MAX phases has not been investigated. The hardness values of TiC_x and TiN_y decrease with increasing vacancy content[13, 15]. In substoichiometric TiN_y, the integrated density of states(DOS) demonstrates that Ti(3*d*)-N(2*p*) bonding states are reduced in the presence of vacancies, leading to a weakened bond strength, shear strength and hardness[40]. Furthermore, it is predicted that the introduction of 12.5% of vacancies in TiN_y significantly reduces its shear stiffness from 190 GPa to less than 150GPa [15], agreeing well with the experimental results [41]. A similar trend has been measured experimentally in TiC_x [13]. For the ternary nitride Ti_2AlN, intuitively, the N vacancies would play a softening role in the mechanical properties.

From Table II, the C_{ij} are reduced due to the weaker M-X bonding, as the concentration of N vacancies is increased. In the hexagonal lattice, the C_{11} is the in-plane elastic response, which is larger than C_{33} derived by the out-of-plane distortion, indicating the average bonding along the in-plane is stronger than the out-of-plane. It is indeed true, somehow determined by the layered structure. However, with higher N deficiency, these two constants become similar as the MAX lattice is becomes more isotropic, which is also shown in Fig. 2. When C_{33} is close to or smaller than C_{11}, it might be feasible to break the M−A−M bonds significantly damaging the M−X−M bonds[42, 43]. This would open a new route to obtaining the derivative 2D MXenes with clean surfaces by means of mechanical exfoliation, instead of the currently chemical etching processes that lead to complicated surface terminal structures and compositions.

Table I . Lattice parameters, Ti-Al and Ti-N distances (R), Wyckoff position of Ti atom (z_{Ti}), and the volume of the unit cell (V), and the formation energy of N vacancy (E_f) of Ti_2AlN_y (y: 0.85-1.05). The relative volume changes in theory are shown in the parenthesis.

N_y	LP **(Å)**	$R_{Ti\text{-}Al}$**(Å)**	$R_{Ti\text{-}N}$**(Å)**	z_{Ti}	V **(Å^3)**	E_f(eV)
$N_{0.88}$(Cal.)	a=2.99669 c=13.6373	2.830	2.084	0.08564	106.074(0.15%)	0.58
$N_{0.85}$(Exp.)	*a* = 2.9875 *c*= 13.6510	2.822	2.090	0.08641	105.506	
$N_{0.91}$(Cal.)	*a=2.99877* *c=13.6255*	2.829	2.084	0.08561	106.129(0.19%)	0.86
$N_{0.90}$(Exp.)	*a* = 2.9891 *c* = 13.632	2.820	2.090	0.08642	105.477	
$N_{0.94}$(Cal.)	*a=2.99754* *c=13.3140*	2.837	2.086	0.08564	106.068(0.14%)	1.14
$N_{0.95}$(Exp.)	*a* = 2.9899 *c*= 13.6189	2.818	2.089	0.08643	105.435	
$N_{1.0}$(Cal.)	*a=2.99889* *c=13.6002*	2.828	2.086	0.08557	105.918	
$N_{1.0}$(Exp.)	*a*=2.99252 *c*= 13.6111	2.818	2.090	0.08643	105.550	
$N_{1.05}$(Exp.)	*a* = 2.9937 *c* =13.6012	2.817	2.090	0.08644	105.566	

While the shear, bulk and Young's moduli are steadily suppressed with the increasing N vacancy concentration, the three moduli show different magnitudes of response of 13.1%, 7.3%, 11.7%, respectively. Experimentally, for pristine Ti_2AlN, the Young's modulus was found to be 278±10GPa, which is in a very good agreement with the result obtained by Resonant Ultrasound Spectroscopy (RUS) on a Ti_2AlN bulk polycrystalline sample (E~277GPa[44]) and 270±20 GPa in another independent measurement by nanoindentation [45]. Note that the calculated E of Ti_2AlN with varying

N vacancies are all falling into the regime between 258.2 and 293.1 GPa, which is in the line with the above measurements. We concluded that the perturbation of mechanical properties by N vacancies are different, and the incompressibility is the least affected.

4.3 *ab initio* calculations

As discussed above, the combination of metallic and ceramic characteristics in MAX phases provide us with opportunities in many applications, where the formation of defects, their dynamics, and the consequences for the mechanical properties are critical. The formation energy for the varying N vacancies E_f was defined as $E_f = (E_v+n\mu_N-E_p)/16$, where E_v denotes the total energy of Ti_2AlN phase with N vacancies, μ_N is the chemical potential for a single N atom as of the $\frac{1}{2}N_2$ gas molecule, E_p stands for the total energy of the pristine Ti_2AlN, and the n is the number of N vacancies in the supercell. Here, we consider the formation energy per unit cell by the division over the size of the supercell, 16. The formation energies of N vacancy in Ti_2AlN are positive, which is similar to the finding of N vacancy in Ti_4AlN_3.[46] It is thus demonstrated that the N vacancies are energetical costly. Moreover, the formation energy of N vacancies in the lower densities are higher than for higher ones.

Having the energetics of the N vacancy formation, we continue to elucidate the mechanical properties and the N vacancies induced changes. Here, we employed two widely used hardness models, $H_{v,Chen}$ [47] and H_v [48] to analyze both defect-free and the deficient Ti_2AlN. Note that Pugh's modulus ratio (k) defined as defined as G/B, as the indicator of a material's brittleness, is usually taken into account, and the above two models are expressed as:

$$H_{v,Chen}=2(k^2G)^{0.585}-3 \quad (4)$$

$$H_{v,Tian}=0.92k^{1.137}G^{0.708} \quad (5)$$

We find that in the above two models the hardness is ~20 GPa and decreases monotonically with greater N deficiency. The reduction magnitude of $H_{v,Chen}$ & $H_{v,Tian}$ are about 16% and 10% from the pristine to the highest N deficient MAX phase. In Eq. (4-5), the exponential of k, G are the key to deduce different slope of the change, but the overview of the moduli and hardness of nitride MAX provides with a clear insight to

the role of the N deficiency. Overall, the drop of the hardness by introducing the N deficiency is not showing a dramatic change in strong contrast to the binary nitrides.

Table II . The calculated elastic constants C_{ij} and the derived shear moduli, G, bulk moduli, B, Young's moduli, E and hardness, H (GPa).

MAX	C_{11}	C_{12}	C_{13}	C_{33}	C_{44}	G	B	E	$H_{v,Chen}$	$H_{v,Tian}$
$Ti_2AlN_{0.88}$	*277.1*	71.8	84.7	277.1	119.1	107.1	145.9	258.2	18.4	24.3
$Ti_2AlN_{0.91}$	*272.1*	74.0	84.9	283.6	121.1	107.8	146.1	259.7	18.6	24.4
$Ti_2AlN_{0.94}$	306.9	72.6	85.1	295.3	126.7	117.1	154.9	280.6	20.3	25.9
Ti_2AlN	*317.9*	71.1	87.8	288.9	133.1	123.2	157.5	293.1	22.0	27.0

It is well known that the bonding in the MAX phases are a combination of covalent, ionic and metallic bonding. To quantify the chemical bonding characters of Ti_2AlN, we compare the ELF in both the N defect free and deficient ($N_{0.90}$) MAX phases in Fig.5. In Fig.5(a), the predominate Ti-N bond shows a mixture of covalency (the blue bridge feature) and ionicity (the red spheres on N that gain extra electrons from Ti). For the Ti-Al bond, there is no evident covalent bonding but near the Ti surface, a red triangle electronic cloud appears and represents the Ti-Al bonding. This strong localized feature illustrates that the Ti-Al bonding more ionic feature, and neither covalent (showing shared electrons) nor a metallic (the level of localization would be about 0.5). Moreover, in Fig. 5(b), the two N vacancies marked by black circles bring about the expansion of Ti-N block because of lack of chemical bonding. We could also observe a slight change within the interlayer spacing where the arrow pointed. It is thus found that the Ti-N block is suppressed in the N-poor regime, and the interlayer interactions are accompanied to be weakened by N vacancies.

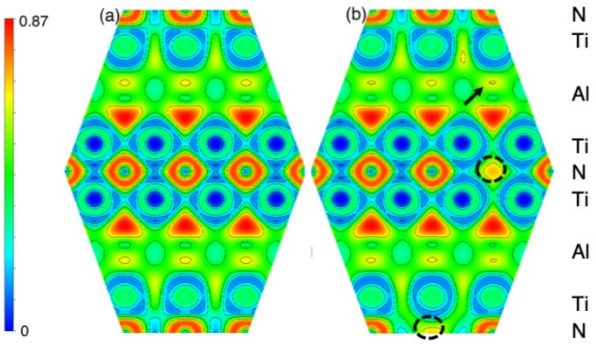

Fig. 5 : 2D cut of the electronic localization function of (a) pristine Ti_2AlN in the miller indices (-111), (b) 2D cut of ELF of $Ti_2AlN_{0.90}$ the view) with the miller indices of (-110) for capturing the defects (marked by spheres) and the changes in the interlayer spacing is marked by arrow. Note that the colour bar on the left represents the level of localization.

We unravel the physical origin behind the electronic properties based on the two series of bonding: Ti(3*d*)-N(2*p*) and Ti(3*d*)-Al(3*p*). First of all, the primary characteristics of the chemical bonding could be deduced from the vacancy free MAX phase: i) the Fermi energy is dominated by Ti(3*d*) states, and the valley shaped DOS near the vicinity of Fermi energy is present. ii) The strong covalent bond is on the Ti(3*d*)-N(2*p*) hybridization is primarily situated between [-7, -6] & [-6, -4] eV with a pseudo-gap about -5.8 eV as a result of the band splitting. iii) The hybridization of Ti(3*d*)-Al(3*p*) states located at -2 and -1.4 eV is weaker intensity and also in higher energy than those of Ti(3*d*)-N(2*p*). In general, for N deficient MAX, the Ti(3*d*)-N(2*p*) hybridization states are become more broadened in contrast to the pristine MAX, due to the band splitting originating from the symmetry breaking. Moreover, although lacking hybridization around -6 eV, the primary Ti-N hybridization peaks between -5 and -4 eV do not change much with lower N. One might also notice that the a splitting width of 0.6 eV is maintained as N_y drops to 0.88, showing a width of about 0.5 eV. For Ti-Al, a similar tendency is also observed, where the two hybridizations near -2 and -1 eV does not experience an absence. We therefore suggest that MAX phases are a unique class of ceramic able to tolerate N deficiency. The methodology of synthesizing the controllable N concentration of MAX phase, would stimulate the development of nitrides MAX and MXenes in substoichiometry. Our results show that N deficiency in ternary MAX phase leads to a slow reduction of the bond lengths and

mechanical properties, particularly the hardness, resulting in smaller changes than the binary TiN_y [15, 41].

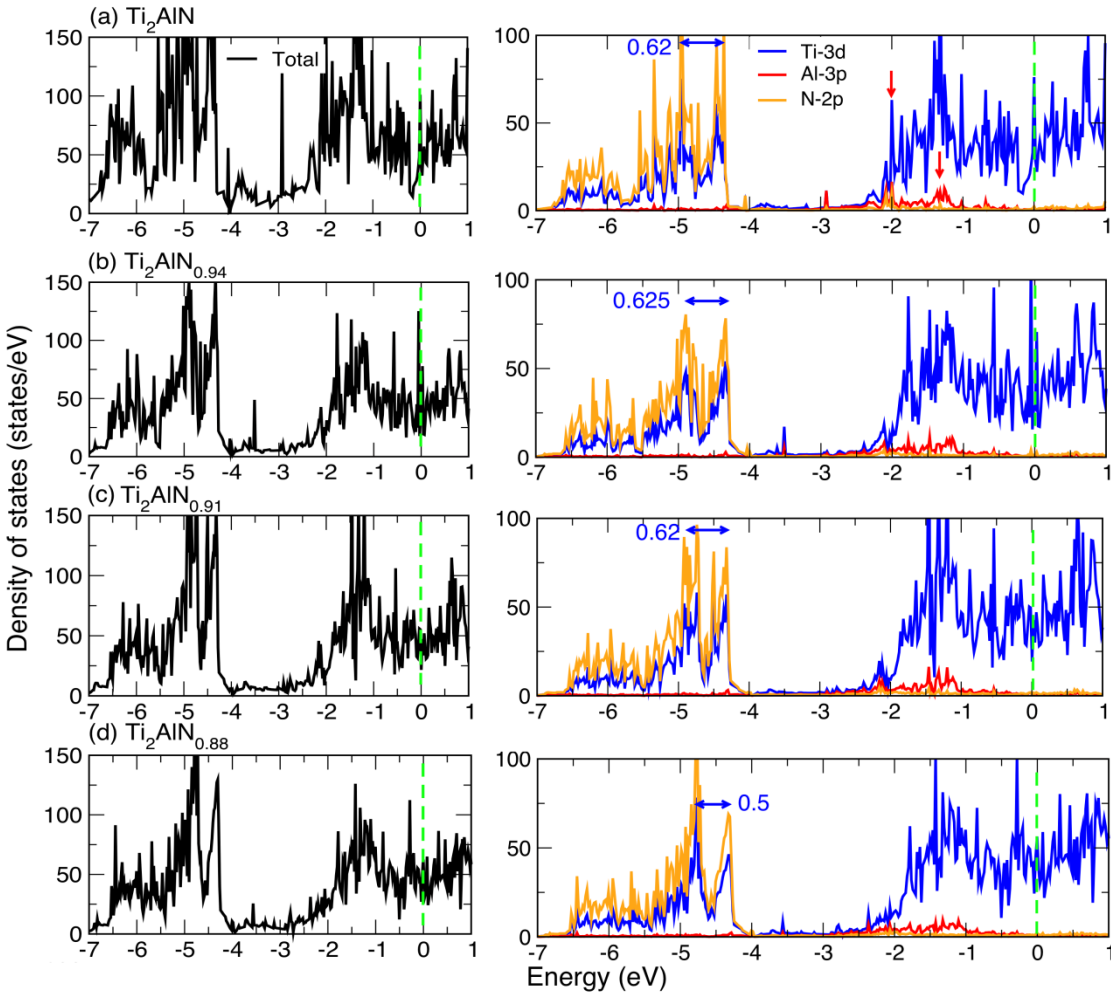

Fig.6 The total and projected DOS of Ti_2AlN and N deficient MAX phases: (a) Ti_2AlN, (b) $Ti_2AlN_{0.94}$, (c) $Ti_2AlN_{0.91}$, (d) $Ti_2AlN_{0.88}$. The total DOS (left side) is represented by black curves, and the projected DOS (right side) for Ti (3*d*), Al (3*p*), and N (2*p*) states is shown in blue, red and orange, respectively.

5. Conclusions:

In order to reveal the relation between the X deficiency and the mechanical properties of MAX phase for potential structural materials and other applications, Ti_2AlN was synthesized with varying N vacancy concentration by pressureless sintering and hot isostatic pressing. XRD and SEM prove that Ti_2AlN could be synthesized with up to 15% N sub-stoichiometry. The reported method will promote the development of N deficient MAX and MXenes. XRD and *ab initio* calculations reveal that the lattice contraction of Ti_2AlN_y is mainly along the *c*-axis. The correspondence between the XRD and calculations indicates that the N vacancies are not highly ordered and are randomly distributed.

The elastic modulus and intrinsic hardness of substoichiometric $Ti_2AlN_{0.9}$ (268GPa and 8.1GPa respectively) are shown to be smaller than that of Ti_2AlN (278GPa and 9.7GPa respectively). Overall the variation of moduli and hardness with up to 10% N deficiency is small in magnitude compared to the stoichiometric materials both experimentally and theoretically, confirming that the Ti_2AlN exhibits a great potential for tolerating N defects. *Ab initio* calculations demonstrate that both Ti-N and Ti-Al bonding exhibit only a slight weakening by the N deficiency.

Acknowledgements

The experimental section was financially supported by the Fundamental Research Funds for the Central Universities (M19JB100020). W.S. and P.K. (initial theory) were supported as part of the Fluid Interface Reactions, Structures and Transport (FIRST) Center, an Energy Frontier Research Center funded by the U.S. Department of Energy, Office of Science, Office of Basic Energy Sciences. This research used resources of the National Energy Research Scientific Computing Center (NERSC), a U.S. Department of Energy Office of Science User Facility operated under Contract No. DE-AC02-05CH11231.

References

1. Wang, J. and Y. Zhou, *Recent progress in theoretical prediction, preparation, and characterization of layered ternary transition-metal carbides.* Annual Review of Materials Research, 2009. **39**: p. 415-443.
2. Barsoum, M.W., *The MN+1AXN phases: A new class of solids: Thermodynamically stable nanolaminates.* Progress in Solid State Chemistry, 2000. **28**(1): p. 201-281.
3. Guitton, A., et al., *Effect of microstructure anisotropy on the deformation of MAX polycrystals studied by in-situ compression combined with neutron diffraction.* Applied Physics Letters, 2014. **104**(24): p. 201.
4. Yu, W., et al., *Solid solution effects in the Ti 2 Al (CxNy) MAX phases: Synthesis, microstructure, electronic structure and transport properties.* Acta Materialia, 2014. **80**: p. 421-434.
5. Bei, G.P., et al., *Compressive Behavior of Ti3AlC2 and Ti3Al0.8Sn0.2C2 MAX Phases at Room Temperature.* Journal of the American Ceramic Society, 2013. **96**(2): p. 567-576.
6. Ward, J., et al., *Corrosion performance of Ti3SiC2, Ti3AlC2, Ti2AlC and Cr2AlC MAX phases in simulated primary water conditions.* Corrosion Science, 2018. **139**: p. 444-453.
7. Radovic, M. and M.W. Barsoum, *MAX phases: Bridging the gap between metals and ceramics.* American Ceramic Society Bulletin, 2013. **92**(3): p. 20-27.
8. W.Barsoum, M., *MAX Phases: Properties of machinable ternary carbides and nitrides.* Wiley-VCH, 2013.
9. Buchholt, K., et al., *Ohmic contact properties of magnetron sputtered Ti3SiC2 on n- and p-type*

4H-silicon carbide. Applied Physics Letters, 2011. **98**(4): p. 8.
10. Wang, Z., et al., *Ohmic contacts on silicon carbide: The first monolayer and its electronic effect.* Physical Review B Condensed Matter, 2009. **80**(24): p. -.
11. Tallman, D.J., et al., *Effect of neutron irradiation on select MAX phases.* Acta Materialia, 2015. **85**: p. 132-143.
12. Ern, V. and A. Switendick, *Electronic band structure of TiC, TiN, and TiO.* Physical Review, 1965. **137**(6A): p. A1927.
13. Pierson, H.O., *Handbook of Refractory Carbides & Nitrides: Properties, Characteristics, Processing and Apps*. 1996: William Andrew.
14. Sun, W., et al., *Self-diffusion of Ti interstitial based point defects and complexes in TiC.* Acta Materialia, 2019. **165**: p. 381-387.
15. Jhi, S.H., et al., *Vacancy hardening and softening in transition metal carbides and nitrides.* Phys Rev Lett, 2001. **86**(15): p. 3348-51.
16. GUO, J.-M., et al., *Effects of TiC and Ti_3AlC_2 Addition on Combustion Synthesis of Ti_3AlC_2 Powders [J].* Journal of Inorganic Materials, 2003. **1**: p. 042.
17. Cabioc'H, T., et al., *Structural investigation of substoichiometry and solid solution effects in Ti2Al(Cx,N1−x)y compounds.* Journal of the European Ceramic Society, 2012. **32**(8): p. 1803-1811.
18. Lofland, S., et al., *Elastic and electronic properties of select< equation> M< sub> 2</sub> AX</equation> phases.* Applied physics letters, 2004. **84**(4): p. 508-510.
19. Barsoum, M.W. and T. El-Raghy, *The MAX phases: unique new carbide and nitride materials.* American Scientist, 2001. **89**(4): p. 336-345.
20. Zhan, C., et al., *Computational Screening of MXene Electrodes for Pseudocapacitive Energy Storage.* The Journal of Physical Chemistry C, 2019. **123**(1): p. 315-321.
21. W. Yu, V.G.-B., T. Cabioc'h and S. Dubois, *synthesis and characterization of $Ti_2Al(C_xN_y)$ solid solutions and related end-members*. 2014, Journal of the American Ceramics society.
22. Pharr, G.M. and A. Bolshakov, *Understanding Nanoindentation Unloading Curves.* Journal of Materials Research, 2002. **17**(10): p. 2660-2671.
23. Woirgard, J. and J.C. Dargenton, *An alternative method for penetration depth determination in nanoindentation measurements.* Journal of Materials Research, 2011. **12**(9): p. 2455-2458.
24. Kresse, G. and J. Furthmüller, *Efficient iterative schemes for ab initio total-energy calculations using a plane-wave basis set.* Physical review B, 1996. **54**(16): p. 11169.
25. Kresse, G. and J. Hafner, *Ab initio molecular-dynamics simulation of the liquid-metal–amorphous-semiconductor transition in germanium.* Physical Review B, 1994. **49**(20): p. 14251.
26. Kresse, G. and J. Hafner, *Ab initio molecular dynamics for open-shell transition metals.* Phys Rev B Condens Matter, 1993. **48**(17): p. 13115-13118.
27. Perdew, J.P., K. Burke, and M. Ernzerhof, *Generalized Gradient Approximation Made Simple.* Physical Review Letters, 1996. **77**(18): p. 3865-3868.
28. Zunger, A., et al., *Special quasirandom structures.* Physical Review Letters, 1990. **65**(3): p. 353.
29. Jordi, P., et al., *Theoretical evaluation of electron delocalization in aromatic molecules by means of atoms in molecules (AIM) and electron localization function (ELF) topological approaches.* Cheminform, 2006. **37**(4): p. 3911-47.
30. Yuan, F., et al., *The pressure induced twisted distortion in flexible oxide Tc2O7.* Crystengcomm, 2015. **18**(2): p. 328-333.
31. Voigt, W., *Lehrbuch der kristallphysik*. Vol. 962. 1928: Teubner Leipzig.

32. Hug, G., *Electronic structures of and composition gaps among the ternary carbides Ti_2MC.* Physical Review B - Condensed Matter and Materials Physics, 2006. **74**(18).
33. Hug, G., M. Jaouen, and M.W. Barsoum, *X-ray absorption spectroscopy, EELS, and full-potential augmented plane wave study of the electronic structure of Ti_2AlC, Ti_2AlN, Nb_2AlC, and $(Ti_{0.5}Nb_{0.5})_2AlC$.* Physical Review B - Condensed Matter and Materials Physics, 2005. **71**(2): p. 024105-1-024105-12.
34. Momma, K. and F. Izumi, *VESTA: A three-dimensional visualization system for electronic and structural analysis.* Journal of Applied Crystallography, 2008. **41**(3): p. 653-658.
35. Fischer-Cripps, A.C., *Nanoindentation*. Vol. 1. 2011: Springer.
36. Tromas, C., et al., *Mechanical Properties of Nanolaminate Ti3SnC2 Carbide Determined by Nanohardness Cartography.* Journal of the American Ceramic Society, 2010. **93**(2): p. 330-333.
37. Bei, G., et al., *Synthesis, Characterization, and Intrinsic Hardness of Layered Nanolaminate Ti3AlC2 and Ti3Al0. 8Sn0. 2C2 Solid Solution.* Journal of the American Ceramic Society, 2011. **95**(1): p. 102-107.
38. Nix, W.D. and H. Gao, *Indentation size effects in crystalline materials: a law for strain gradient plasticity.* Journal of the Mechanics and Physics of Solids, 1998. **46**(3): p. 411-425.
39. M.W. BARSOUM, M.A., and T. EL-RAGHY, *Processing and characterization of Ti2AlC, Ti2AlN and Ti2AlC0.5N0.5.* METALLURGICAL AND MATERIALS TRANSACTIONS A, 2000. **31A**.
40. Magnuson, M., et al., *Bonding mechanism in the nitrides Ti2AlN and TiN: an experimental and theoretical investigation.* Phys.rev.b, 2007. **76**(19): p. 195127.
41. Jiang, X., et al., *Elastic constants and hardness of ion‐beam‐sputtered TiNx films measured by Brillouin scattering and depth‐sensing indentation.* Journal of applied physics, 1991. **69**(5): p. 3053-3057.
42. Khazaei, M., et al., *Trends in electronic structures and structural properties of MAX phases: a first-principles study on M(2)AlC (M = Sc, Ti, Cr, Zr, Nb, Mo, Hf, or Ta), M(2)AlN, and hypothetical M(2)AlB phases.* J Phys Condens Matter, 2014. **26**(50): p. 505503.
43. Khazaei, M., et al., *The effect of the interlayer element on the exfoliation of layered Mo2AC (A = Al, Si, P, Ga, Ge, As or In) MAX phases into two-dimensional Mo2C nanosheets.* Science & Technology of Advanced Materials, 2014. **15**(1): p. 1-7.
44. Radovic, M., A. Ganguly, and M. Barsoum, *Elastic properties and phonon conductivities of Ti~ 3Al (C~ 0~.~ 5, N~ 0~.~ 5)~ 2 and Ti~ 2Al (C~ 0~.~ 5, N~ 0~.~ 5) solid solutions.* JOURNAL OF MATERIALS RESEARCH-PITTSBURGH THEN WARRENDALE-, 2008. **23**(6): p. 1517.
45. Joelsson, T., et al., *Single-crystal< equation>< font face='verdana'> Ti< sub> 2</sub>< font face='verdana'> Al< font face='verdana'> N</equation> thin films.* Applied physics letters, 2005. **86**(11): p. 111913-111913-3.
46. Music, D., R. Ahuja, and J.M. Schneider, *Theoretical study of nitrogen vacancies in Ti4AlN3.* 2005. **86**(3): p. 235108.
47. Chen, X.Q., et al., *Modeling hardness of polycrystalline materials and bulk metallic glasses.* Intermetallics, 2011. **19**(9): p. 1275-1281.
48. Tian, Y., X. Bo, and Z. Zhao, *Microscopic theory of hardness and design of novel superhard crystals.* International Journal of Refractory Metals & Hard Materials, 2012. **33**(33): p. 93-106.